NACA RM E54G28

RESEARCH MEMORANDUM

EFFECTS OF SECONDARY-AIR FLOW ON ANNULAR BASE FORCE OF A SUPERSONIC AIRPLANE

By Donald J. Vargo

Lewis Flight Propulsion Laboratory
Cleveland, Ohio

NATIONAL ADVISORY COMMITTEE
FOR AERONAUTICS

WASHINGTON
October 11, 1954

NACA RM E54G28

NATIONAL ADVISORY COMMITTEE FOR AERONAUTICS

RESEARCH MEMORANDUM

EFFECTS OF SECONDARY-AIR FLOW ON ANNULAR BASE FORCE OF A SUPERSONIC AIRPLANE

By Donald J. Vargo

SUMMARY

The effect of base bleed on the base force of a supersonic-interceptor model was investigated in the Lewis 8- by 6-foot supersonic wind tunnel. Two groups of fixed-geometry nozzles and shroud combinations simulating double-iris-type configurations were evaluated over a range of secondary to primary exit-diameter ratios from 1.12 to 1.65. The shroud lengths varied from 0.09 nozzle diameter ahead to 0.19 nozzle diameter aft of the plane of the nozzle exit. Secondary- to primary-flow ratios reaching 10 percent were investigated for primary pressure ratios up to approximately 16 at Mach numbers of 0.6, 1.5, 1.6, 1.7, and 2.0.

In general, base pressures greater than ambient were obtained at the engine operating pressure ratios of the primary nozzle. This effective thrust was further increased with increases in secondary bleed flow. Unless the secondary air is used for purposes other than bleeding into the base region or is taken from the low-energy boundary layer, the penalty of taking the air aboard is too great to be practical when compared with the thrust increases obtained.

INTRODUCTION

The blunt annular region between the exit nozzle of a jet engine and the afterbody skin enclosing the nozzle is subject to a force generally referred to as base drag. In terms of the total vehicle drag, the base drag may assume varying degrees of importance, depending upon the particular nozzle-afterbody configuration, the stream velocity, and the nozzle pressure ratio.

Previously reported work (refs. 1 to 4) has indicated the magnitude and variation of base force with body configuration and operating conditions. In particular, it has been demonstrated that the base drag may be reduced appreciably by bleeding small amounts of air into the base region (refs. 1 to 3). This introduction of mass flow into the base

region not only tends to increase the local static pressure by reducing the free-stream expansion in the region of the afterbody but also contributes a thrust to the configuration. Previous investigations of these effects were done with idealized configurations representing general design trends. As part of a program to evaluate a proposed interceptor aircraft, data were taken on the effect of flow exiting through the annular base on base force at free-stream Mach numbers of 0.6, 1.5, 1.6, 1.7, and 2.0. Two types of afterbody-nozzle configurations were tested at nozzle pressure ratios from jet-off to greater than 16. Secondary mass flows were varied from 0.4 percent to approximately 10 percent of the primary-nozzle mass flow. Some data were also taken on the influence of the primary-jet temperature on the base force.

SYMBOLS

The following symbols are used in this report:

A	area, sq ft
C_j	secondary-jet-thrust coefficient, $\frac{q_0 C_p A_b + m_s V_s}{q_0 A_{max}}$
C_n	secondary-net-thrust coefficient, $\frac{q_0 C_p A_b + m_s V_s - m_s V_0}{q_0 A_{max}}$
C_p	pressure coefficient, $(p - p_0)/q_0$
H	total pressure, lb/sq ft
M	Mach number
m	mass flow, slugs/sec
p	static pressure, lb/sq ft
q	dynamic pressure, $\frac{\gamma}{2} pM^2$, lb/sq ft
S	distance between end of nozzle and end of shroud (measured positive when shroud is longer than nozzle)
S/D_p	spacing ratio
T	total temperature, $^{\circ}R$
V	velocity, ft/sec
W	nozzle weight flow, lb/sec

γ ratio of specific heats

$\omega\sqrt{\tau}$ ratio of secondary to primary weight-flow parameter, $\frac{W_s\sqrt{T_s}}{W_p\sqrt{T_p}}$

Subscripts:

b base annulus

max maximum body cross section, 0.336 sq ft

p primary

s secondary

0 free stream

APPARATUS AND PROCEDURE

The basic apparatus employed was a 1/10-scale model of the fuselage of a delta-wing supersonic interceptor. The body supports simulated the wings and served as hollow struts for the ducting of high-pressure air into the model (fig. 1(a)). The method of measuring weight flows, temperatures, and pressures of primary and secondary flows was essentially the same as that given in reference 5. In summary, the rate of air flow to the model was measured by an A.S.M.E. type orifice in the air supply line. After entering the model, this internal air was turned 90° and passed through the primary- and secondary-flow passages. Secondary-air flow was controlled by a sliding-valve arrangement at the perforated ring (fig. 1(b)), which had been given a bench-test calibration. In order to avoid possible formation of condensation shocks in the nozzle, the air was preheated to approximately 700° R prior to entering the model. The hot-flow data were obtained by burning fuel in a can-type burner installed in the model afterbody. Primary-flow temperatures could thus be increased up to approximately 3000° R.

Details of the internal and external geometry of the afterbody section are shown in figure 1(b). Also indicated is the method of attachment of the shroud-nozzle combination to the assymmetric afterbody. Variable-geometry nozzle-shroud combinations were simulated with two series of fixed-geometry configurations. The first group represents a two-position nozzle of relatively rapid convergence and will be referred to as group A (fig. 2(a)). The remaining nozzles simulate various positions of a double-iris arrangement having relatively gradual nozzle convergence and will be referred to as group B (fig. 2(b)).

A method of configuration identification is used in which the letter indicates the configuration group. The first number is the diameter ratio (ratio of shroud diameter to primary-nozzle diameter D_s/D_p) and the second number is the spacing ratio (distance between end of shroud and end of primary nozzle divided by primary-nozzle diameter S/D_p). In group A, figure 2(a), configurations A 1.12-0.057 and A 1.65-0 represent the nonafterburning nozzle position with two alternative shrouds. Configuration A 1.24-0 represents the afterburning nozzle position. Configuration B 1.39-0.09 represents the nonafterburning position of the group B nozzles, figure 2(b), while configurations B 1.27-(-0.010) and B 1.18-(-0.06) represent various afterburning positions corresponding to increases in flight Mach number to 2.0. Nozzle B 1.18-(-0.14) is a modified version of nozzle B 1.13-(-0.19), wherein the slight divergence at the exit has been replaced by a straight section.

Internal static-pressure measuring stations are shown in figure 1(b). Inasmuch as the secondary passage area was large and the velocity low, the static orifices near the secondary-air inlet holes were assumed to read essentially total pressure P_s. The assumption of isentropic flow to the exit was checked by installing total-pressure tubes in the region between the shroud and the nozzle for several runs. Discrepancies were generally small and are not believed to be significant. A slight correction was applied to the secondary-air flow to account for leakage through the small gap between the shroud and the afterbody. One-dimensional approximations were used to calculate the total secondary exit momentum from the calibrated mass flow and the static pressure measured at the rearward station indicated in figure 1(b).

Similar calculations were made for the hot-flow data except that, for the primary nozzle, the weight of the fuel was added to the air flow to obtain the total primary weight flow. Reynolds number range in the test section varied approximately from 4×10^6 to 5×10^6 per foot of tunnel length.

RESULTS AND DISCUSSION

Usually the force applied to a base region is referred to as base drag. However, since for the configurations considered in this report an exit flow momentum is added to the conventional base drag definition, this base force will be designated as secondary-jet-thrust coefficient C_j. Similarly, secondary-net-thrust coefficient C_n is used to define the difference between the total momentum at the secondary exit C_j and the free-stream momentum of the secondary mass flow. Figures 3 and 4 illustrate the variation of secondary jet thrust with Mach number, nozzle pressure ratio, and amount of secondary base bleed for nozzle groups A and B. Primary-nozzle pressure ratios for a representative jet engine are indicated by an arrow on the abscissas of the figures.

For both nozzle groups the increase of base force with secondary flow is in agreement with previously published results (ref. 4). Differences in base force for a jet-off condition ($H_p/p_0 = 1$) are generally small for the group A configurations (fig. 3). However, at Mach 1.7, configuration A 1.12-0.057, despite having a greater shroud convergence angle, definitely has a higher thrust base force than either configuration A 1.24-0 or configuration A 1.65-0. This higher thrust base force is, in part, attributable to the smaller diameter ratio; previously established results (fig. 6 of ref. 4) have indicated a rising base pressure with decreasing diameter ratio.

With primary flow and at similar values of the secondary-flow parameter $\omega\sqrt{\tau}$, the highest secondary jet thrust for group A nozzles was generally obtained with configuration A 1.24-0. Since an increase in base thrust with decreasing nozzle convergence has been demonstrated in reference 6, this result is probably associated with the fact that the nozzle of configuration A 1.24-0 induced the least convergence of the primary exit flow.

In contrast with the trend observed for configuration A 1.12-0.057, for jet-on conditions, the group B configurations having the lowest shroud angles generally had the highest base pressure. This indicates that, with the given afterbody, lower-angle shroud extensions cause greater compression of the external flow and result in higher local static pressures in the region of the base. Inasmuch as the magnitude of the base pressure depends greatly on the pressures experienced along the shroud, these trends might be expected (ref. 7).

Data were taken with both series of nozzle-afterbody configurations at primary-nozzle temperatures ranging from 700° to ≈ 3000° R. Since the hot-flow data are limited, a complete analysis was not attempted. However, addition of heat to the primary stream resulted in slightly higher base pressures than equivalent cold-flow data. These slight differences may be caused by the effect of a change in specific heats, as was noted in reference 8.

The variation of the bleed pressure ratio H_s/p_0 with the base bleed-flow parameter and the primary-nozzle pressure ratio is indicated in figures 5 and 6. Over the Mach number range investigated, the trends are similar for all configurations of both nozzle groups. For any one nozzle configuration, an increase in free-stream Mach number results in a decrease in the bleed pressure ratio for constant values of primary pressure ratio and weight-flow parameter. Since the bleed flow was small and at a low pressure ratio, it remained unchoked. Consequently, an increase in M_0, which for these configurations lowers the static pressure in the base region, requires a corresponding decrease in secondary total pressure H_s to maintain the same value of the weight-flow parameter $\omega\sqrt{\tau}$.

[redacted]

This reduction in H_s is interpreted as lowering the base bleed pressure ratio.

A comparison of the nonejector base bleed configurations of this report with ejector configurations formed by extending the shrouds (ref. 5) indicates that the nonejectors require lower secondary pressure ratios H_s/p_0 to pump a given secondary-flow parameter $\omega\sqrt{\tau}$ than did similar ejector configurations.

Previously presented data of this report have been cross-plotted in figure 7 to show the effect of increasing secondary weight flow on secondary jet thrust at typical engine operating pressure ratios. In addition, free-stream inlet momentum of secondary air was subtracted from the secondary jet thrust C_j to give a net base thrust C_n. Increasing the secondary-weight-flow parameter $\omega\sqrt{\tau}$ from 0.005 to 0.05 increased the secondary-jet-thrust coefficients at supersonic speeds by amounts corresponding to a maximum of 7 percent of a representative airplane drag. However, the curves of net-base-thrust coefficient indicate that the loss in free-stream inlet momentum is too great a penalty to pay for the amount of base-thrust increase obtained. Previous work (ref. 1) with a high-base-drag configuration indicated that scooping base bleed air from the inner layers of the boundary layer gave approximately a 7.5-percent reduction of total model fuselage drag. If, as intended for this configuration, the air is taken aboard for purposes of engine and afterburner cooling, then increases in thrust may be realized by releasing this air in the base regions. The curves of figure 7 may be conservative, since the secondary flow was assumed to be at free-stream temperature. In an actual case, the secondary flow will be at a higher temperature than the external stream, thereby reducing secondary weight flow at constant weight-flow ratio parameter $\omega\sqrt{\tau}$ and consequently decreasing the inlet momentum penalty.

3397

SUMMARY OF RESULTS

The effect of secondary-air flow on the base force of the two groups of nozzle-shroud configurations was investigated over a range of pressure ratios from jet-off to greater than 16 at free-stream Mach numbers of 0.6, 1.5, 1.6, 1.7, and 2.0. For this range of variables, the following conclusions were reached:

1. For both series of nozzle configurations, an increase in the flow out of the base annulus caused a corresponding increase in base thrust. In general, for one of the nozzle families investigated, the configurations having the lowest shroud angles (measured with respect to the body center line) had the highest base thrust.

2. At a constant primary-pressure ratio, an increase in free-stream Mach number caused a decrease in model base pressure. Since the amount of secondary flow was small and at a low secondary total pressure, it remained unchoked and subject to external conditions. Consequently, increasing the free-stream Mach number lowered the base pressure and, in turn, decreased the required secondary total pressure to maintain the same value of the weight-flow parameter.

3. In general, base pressures greater than ambient were obtained at the engine operating pressure ratios of the primary nozzle. At these pressure ratios, increasing the secondary flow from 0.5 to 5 percent of the primary flow increased the base thrust in amounts corresponding to a maximum of 7 percent of the total drag of a supersonic airplane. However, unless the secondary air is used for purposes other than bleeding into the base region or is taken from the low-energy boundary layer, the penalty of taking the air aboard is too great to be practical when compared with the thrust increases obtained.

Lewis Flight Propulsion Laboratory
National Advisory Committee for Aeronautics
Cleveland, Ohio, July 30, 1954

REFERENCES

1. Cortright, Edgar M., Jr., and Schroeder, Albert H.: Preliminary Investigation of Effectiveness of Base Bleed in Reducing Drag of Blunt-Base Bodies in Supersonic Stream. NACA RM E51A26, 1951.

2. Hebrank, W. H., Scanland, T. S., Platou, A. S., and Hicks, B. L.: The Effects on Base Pressure of Air Ejection from the Base of a Model Projectile at $M_0 = 1.7$ - Partial Evaluation of the External Ram Jet Principles. Memo. Rep. No. 539, Ballistic Res. Labs., Aberdeen Proving Ground (MD), Aug. 1951. (Proj. No. TB3-0110V, Res. and Dev. Div., Ord. Corps.)

3. Cortright, Edgar M., Jr., and Schroeder, Albert H.: Investigation at Mach Number 1.91 of Side and Base Pressure Distributions over Conical Boattails without and with Jet Flow Issuing from Base. NACA RM E51F26, 1951.

4. Cortright, Edgar M., Jr., and Kochendorfer, Fred D.: Jet Effects on Flow over Afterbodies in Supersonic Stream. NACA RM E53H25, 1953.

5. Allen, John L.: Pumping Characteristics for Several Simulated Variable-Geometry Ejectors with Hot and Cold Primary Flow. NACA RM E54G15, 1954.

6. Vargo, Donald J., and Englert, Gerald W.: Effect of Nozzle Contour on Drag of Parabolic Afterbodies. NACA RM E54D02, 1954.

7. Chapman, Dean R.: An Analysis of Base Pressure at Supersonic Velocities and Comparison with Experiment. NACA Rep. 1051, 1951. (Supersedes NACA TN 2137.)

8. Hearth, Donald P., and Wilcox, Fred A.: Thrust and Drag Characteristics of a Convergent-Divergent Nozzle with Various Exhaust Jet Temperatures. NACA RM E53L23b, 1954.

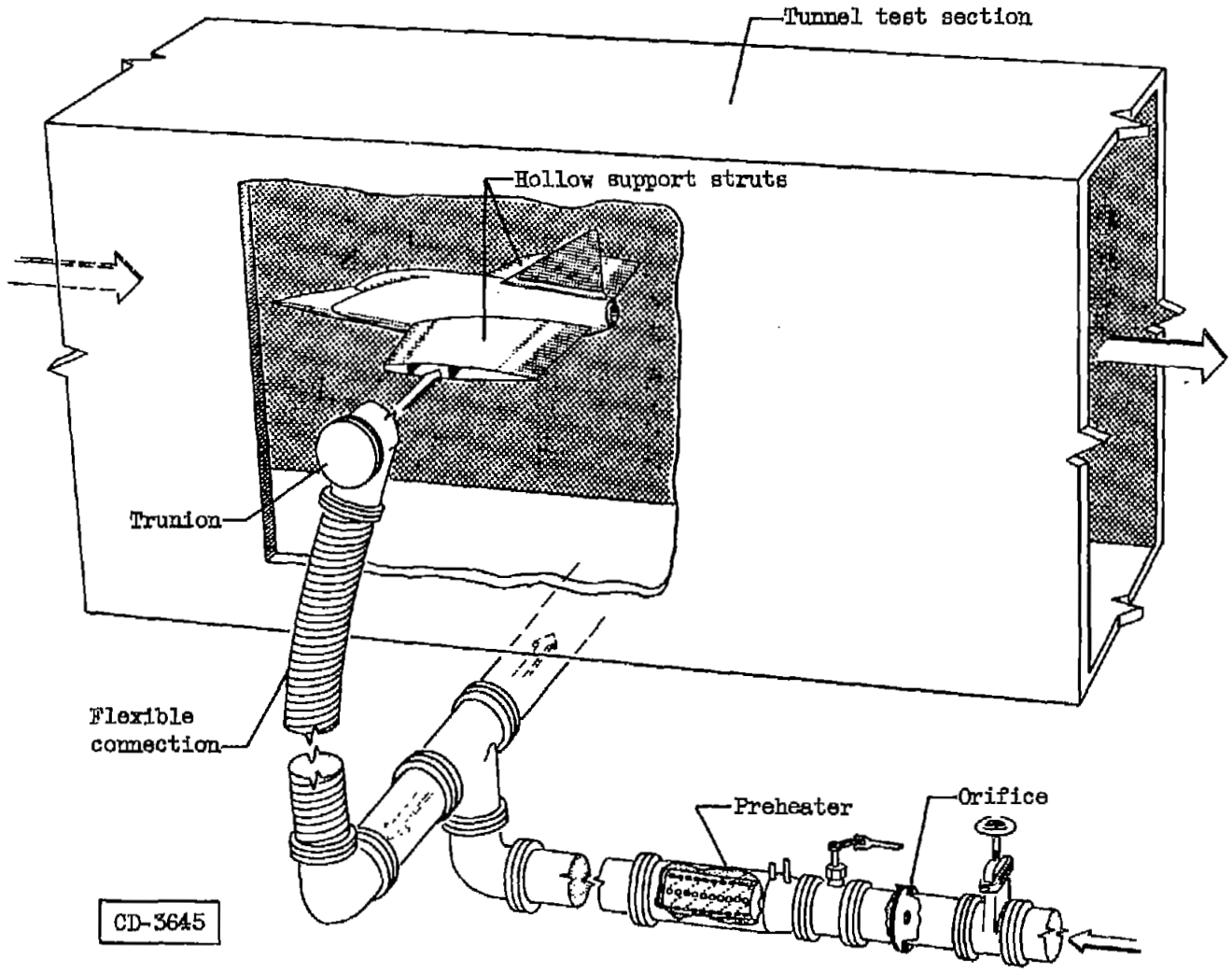

(a) Schematic drawing of jet-exit model in 8- by 6-foot test section.

Figure 1. - Experimental apparatus.

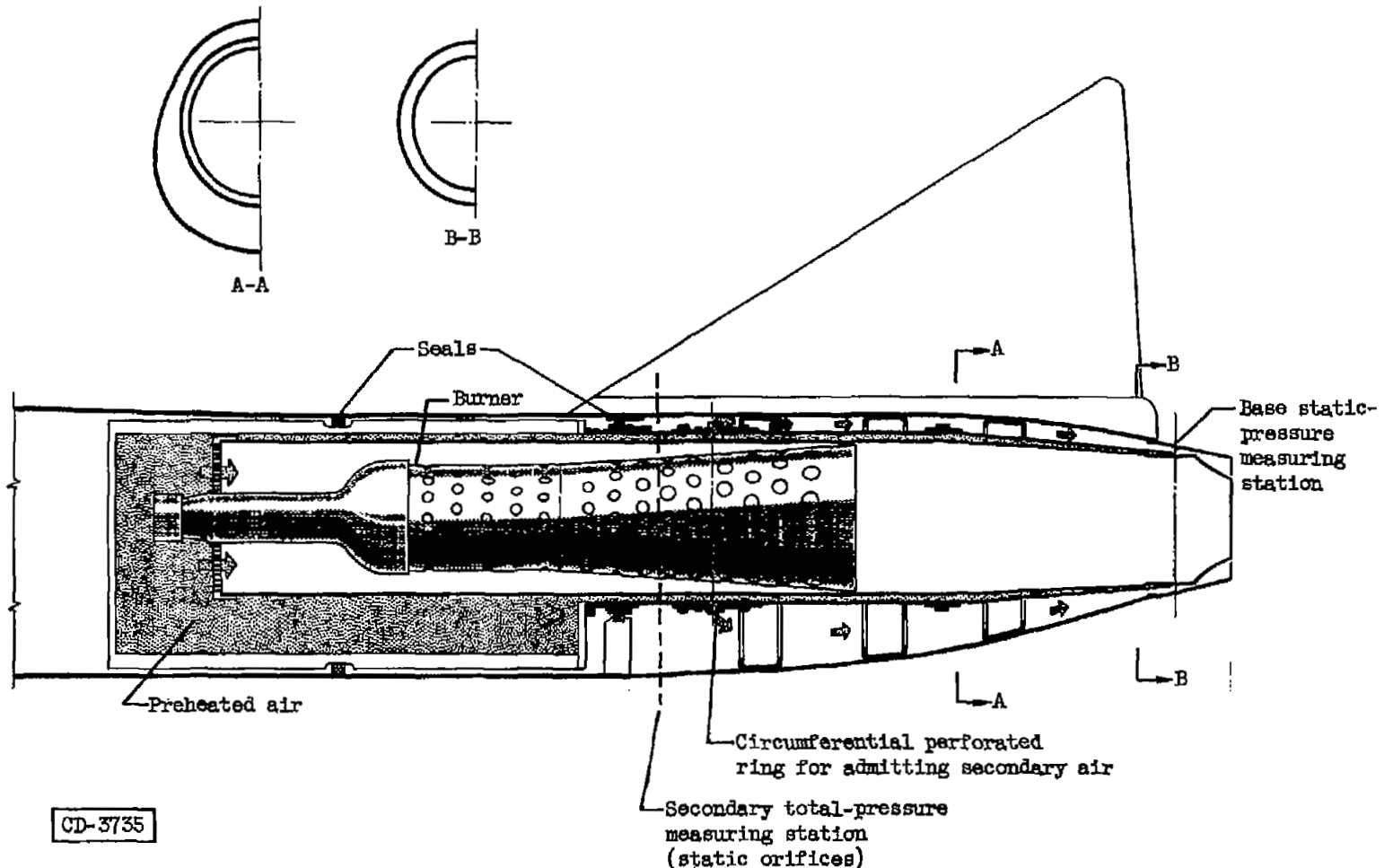

(b) Schematic diagram of aft portion of 1/10-scale model.

Figure 1. - Concluded. Experimental apparatus.

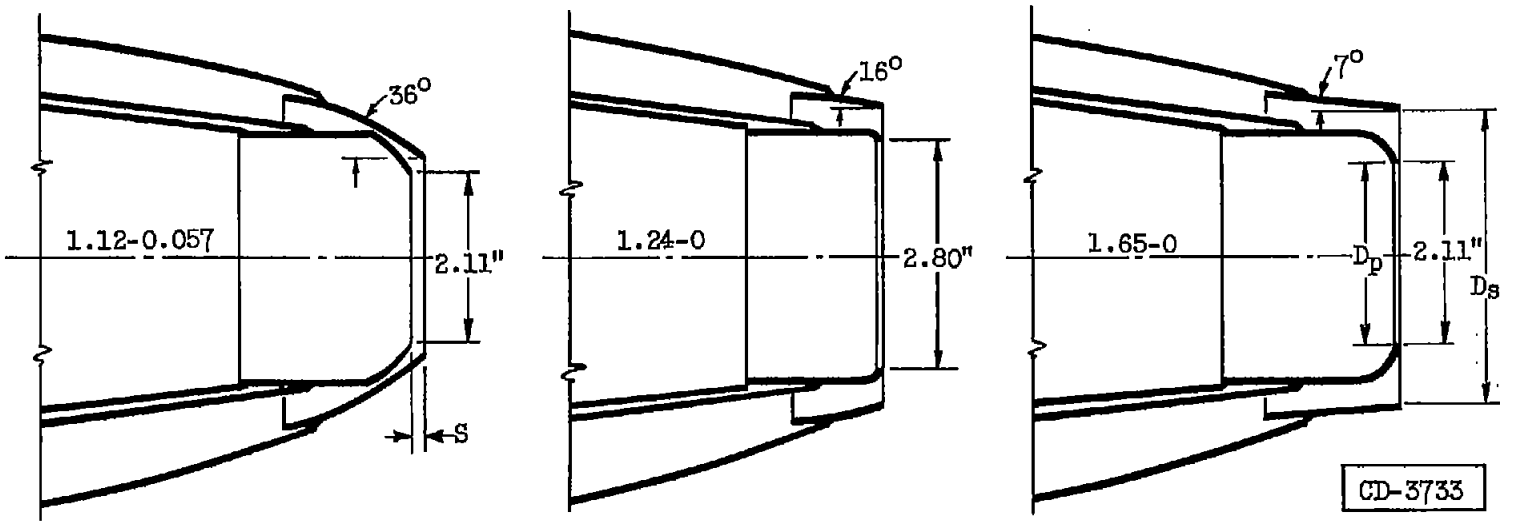

(a) Group A nozzles.

Figure 2. - Schematic of nozzle geometry.

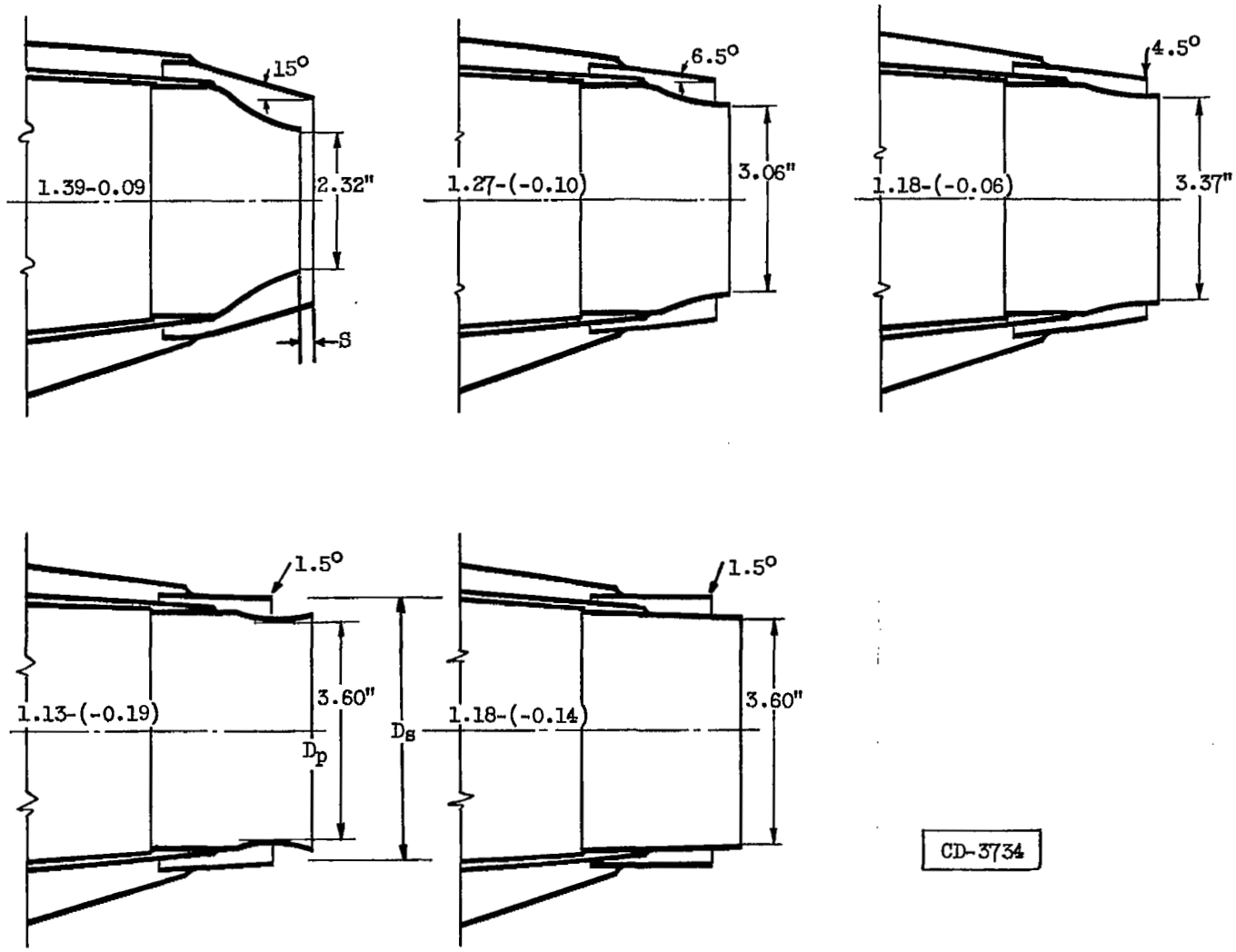

(b) Group B nozzles.

Figure 2. - Concluded. Schematic of nozzle geometry.

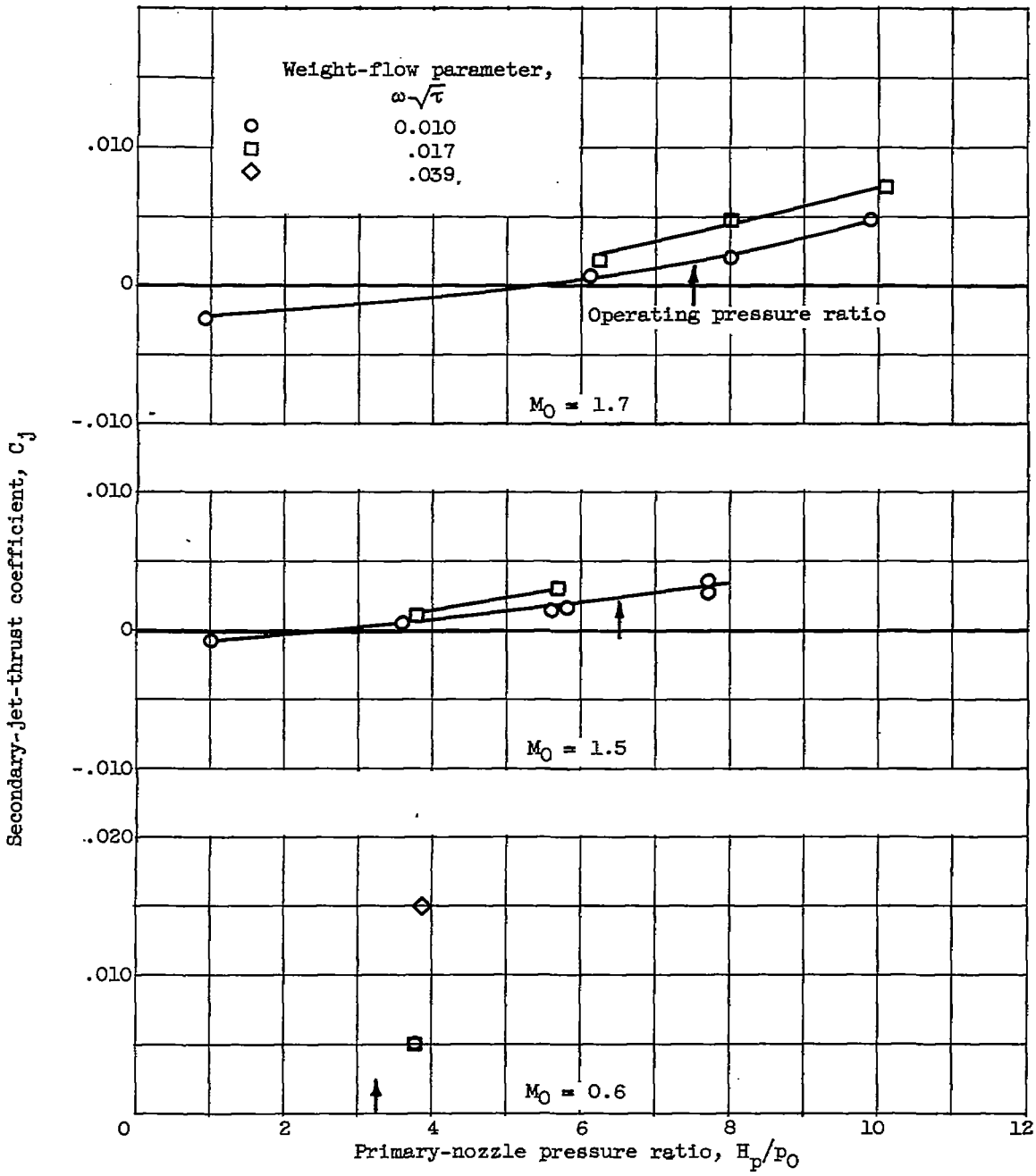

(a) Configuration 1.12-0.057.

Figure 3. - Secondary-jet-thrust coefficient for group A nozzles.

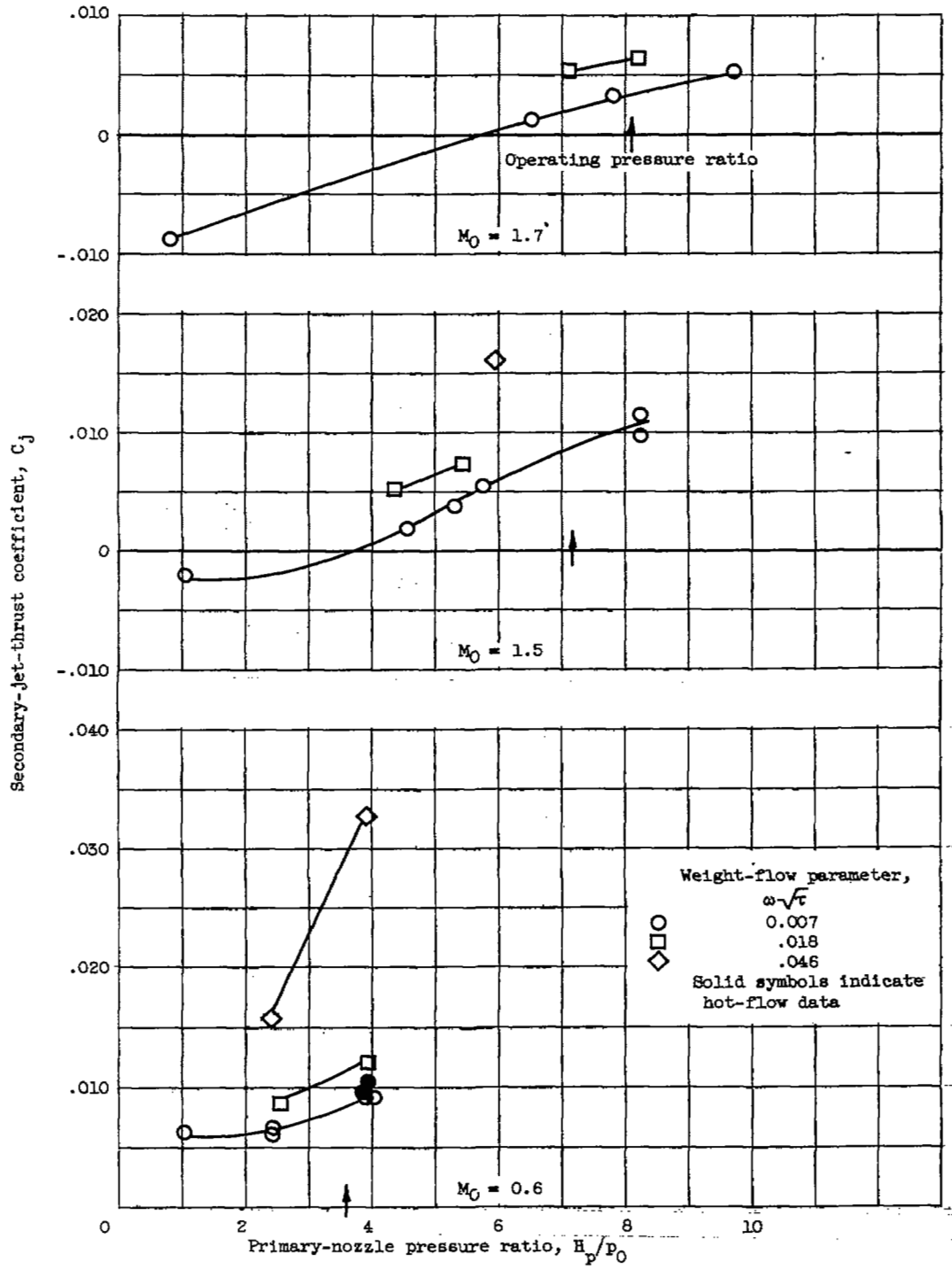

(b) Configuration 1.24-0.

Figure 3. - Continued. Secondary-jet-thrust coefficient for group A nozzles.

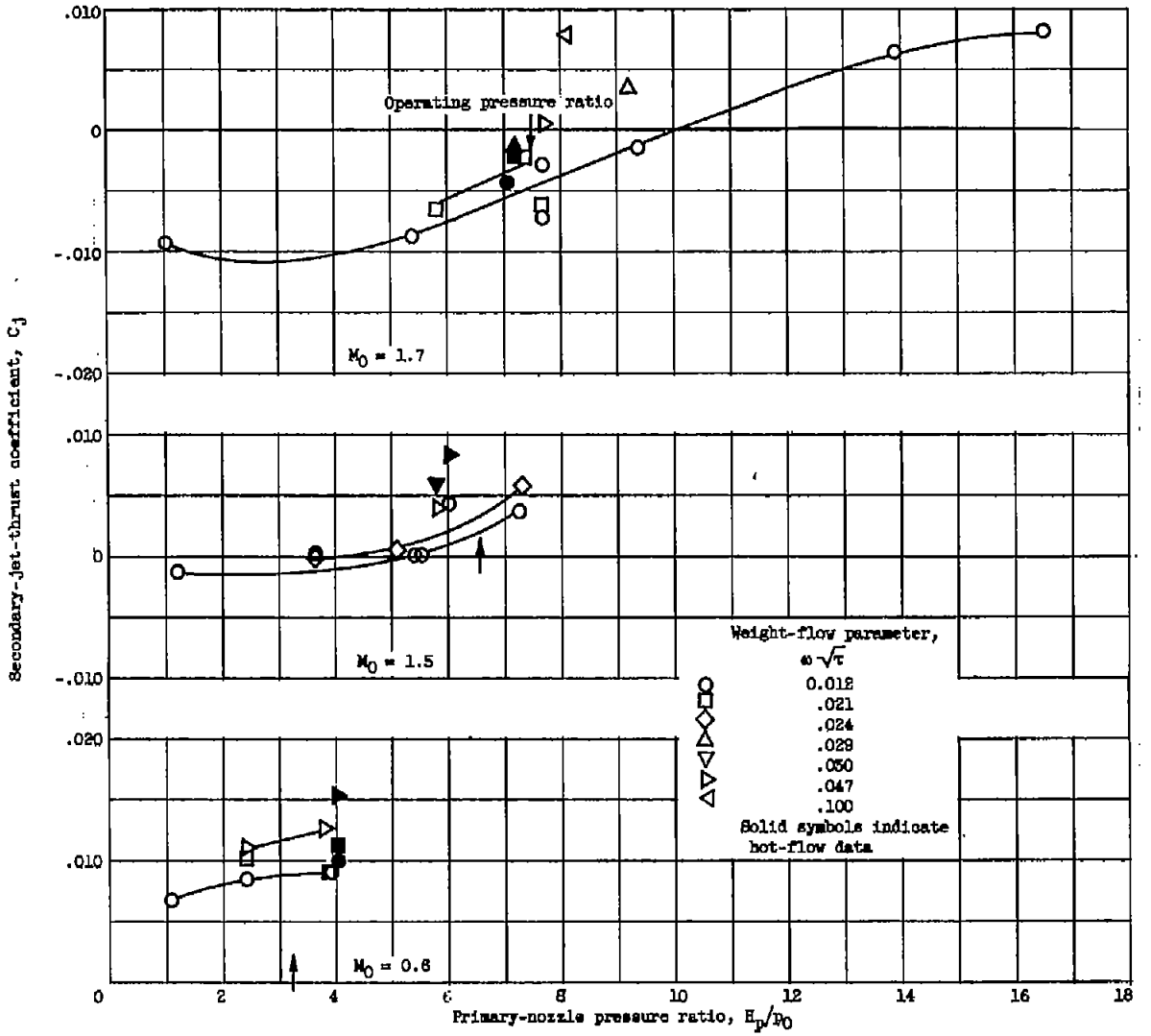

(c) Configuration 1.65-0.

Figure 3. - Concluded. Secondary-jet-thrust coefficient for group A nozzles.

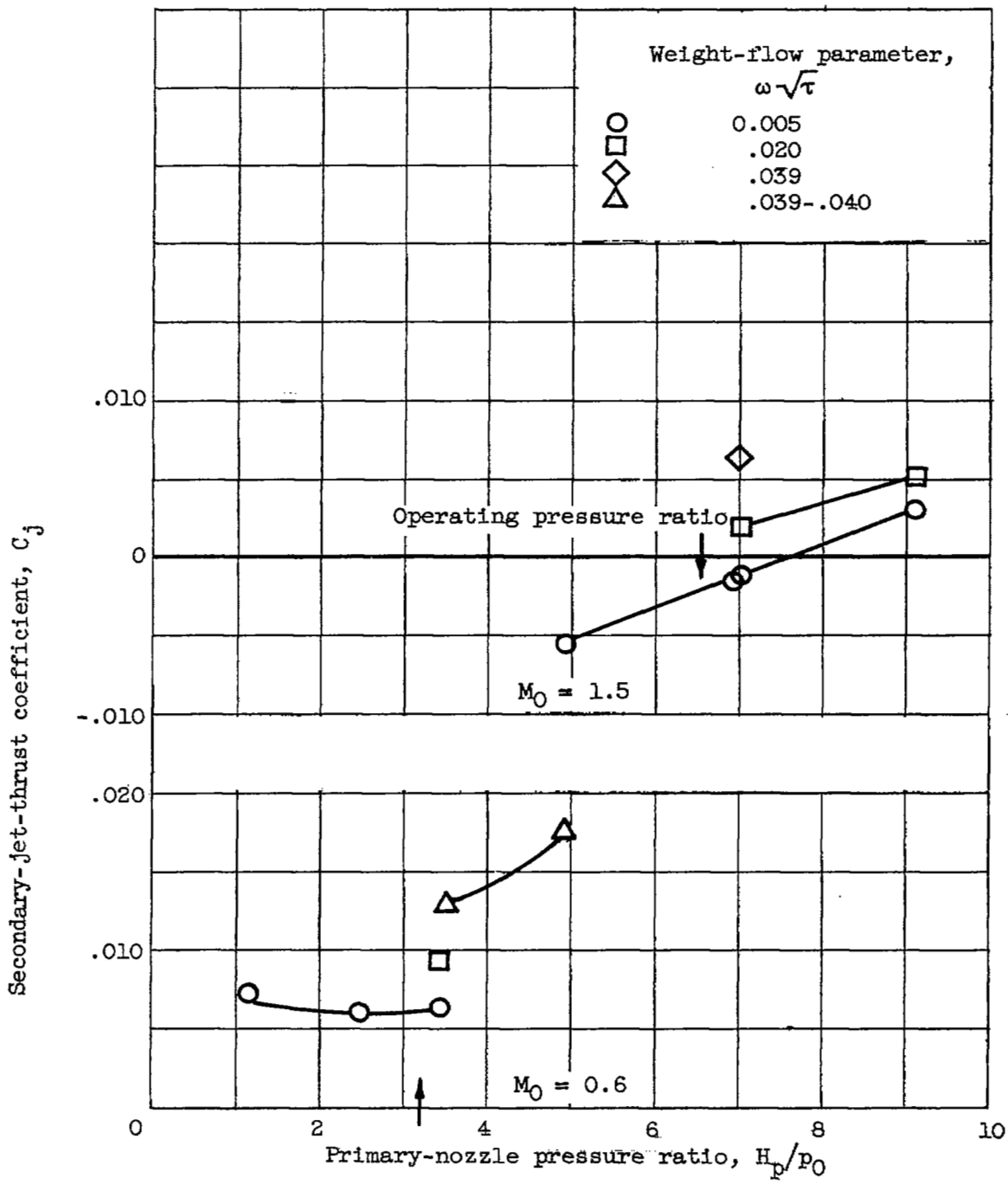

(a) Configuration 1.39-0.09.

Figure 4. - Secondary-jet-thrust coefficient for group B nozzles.

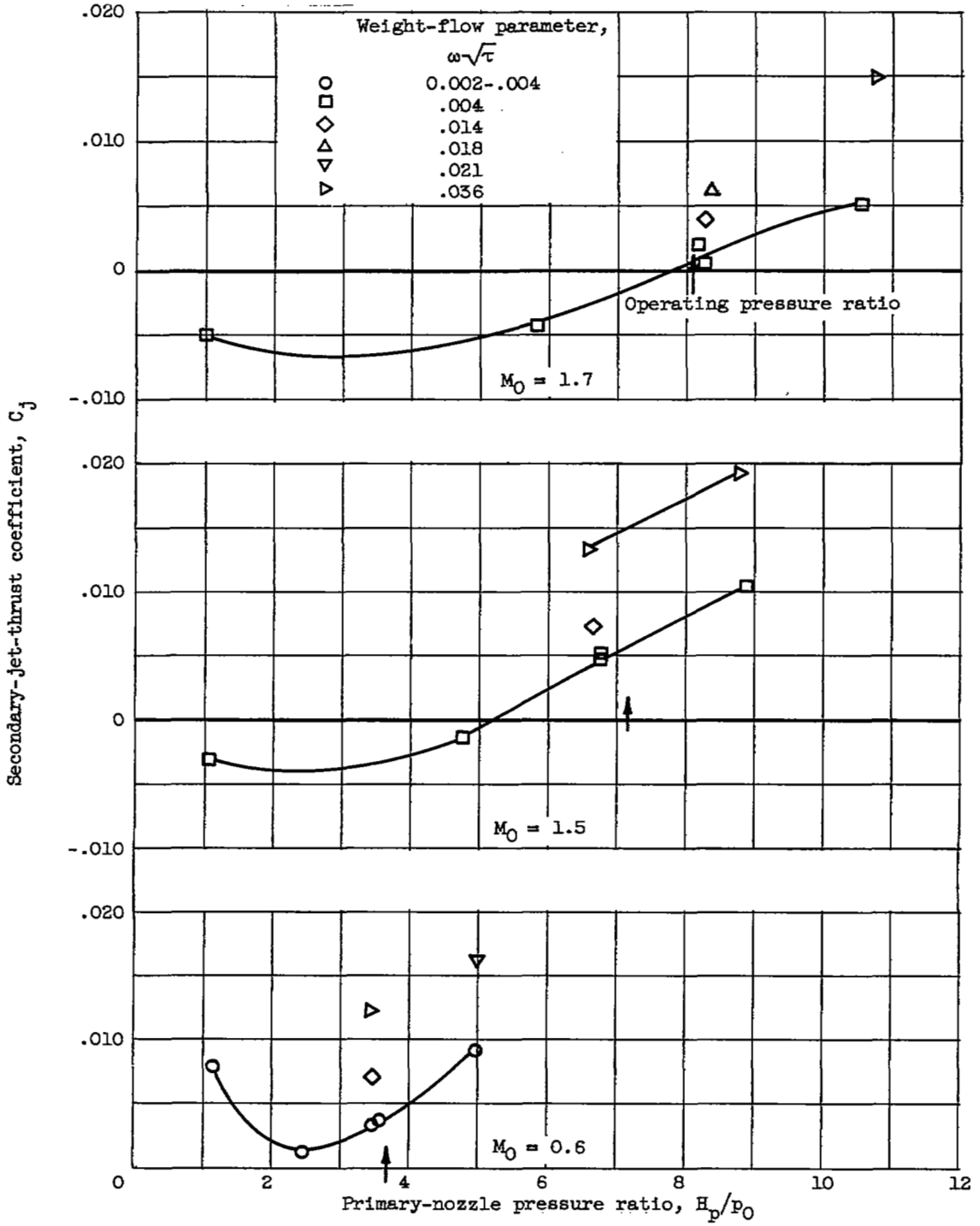

(b) Configuration 1.27-(-10).

Figure 4. - Continued. Secondary-jet-thrust coefficient for group B nozzles.

[redacted]

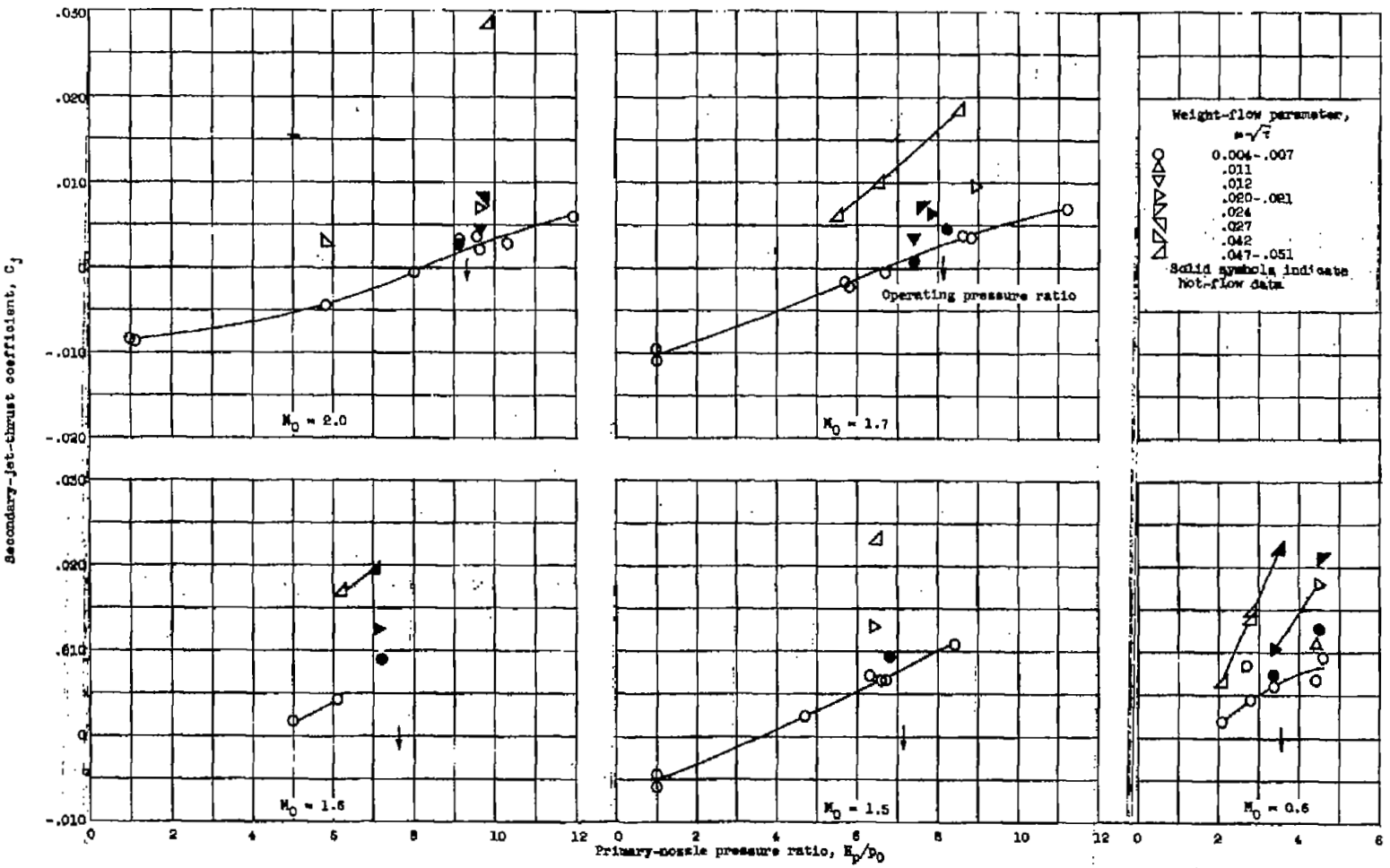

(c) Configuration 1.18-(-0.06).

Figure 4. - Continued. Secondary-jet-thrust coefficient for group B nozzles.

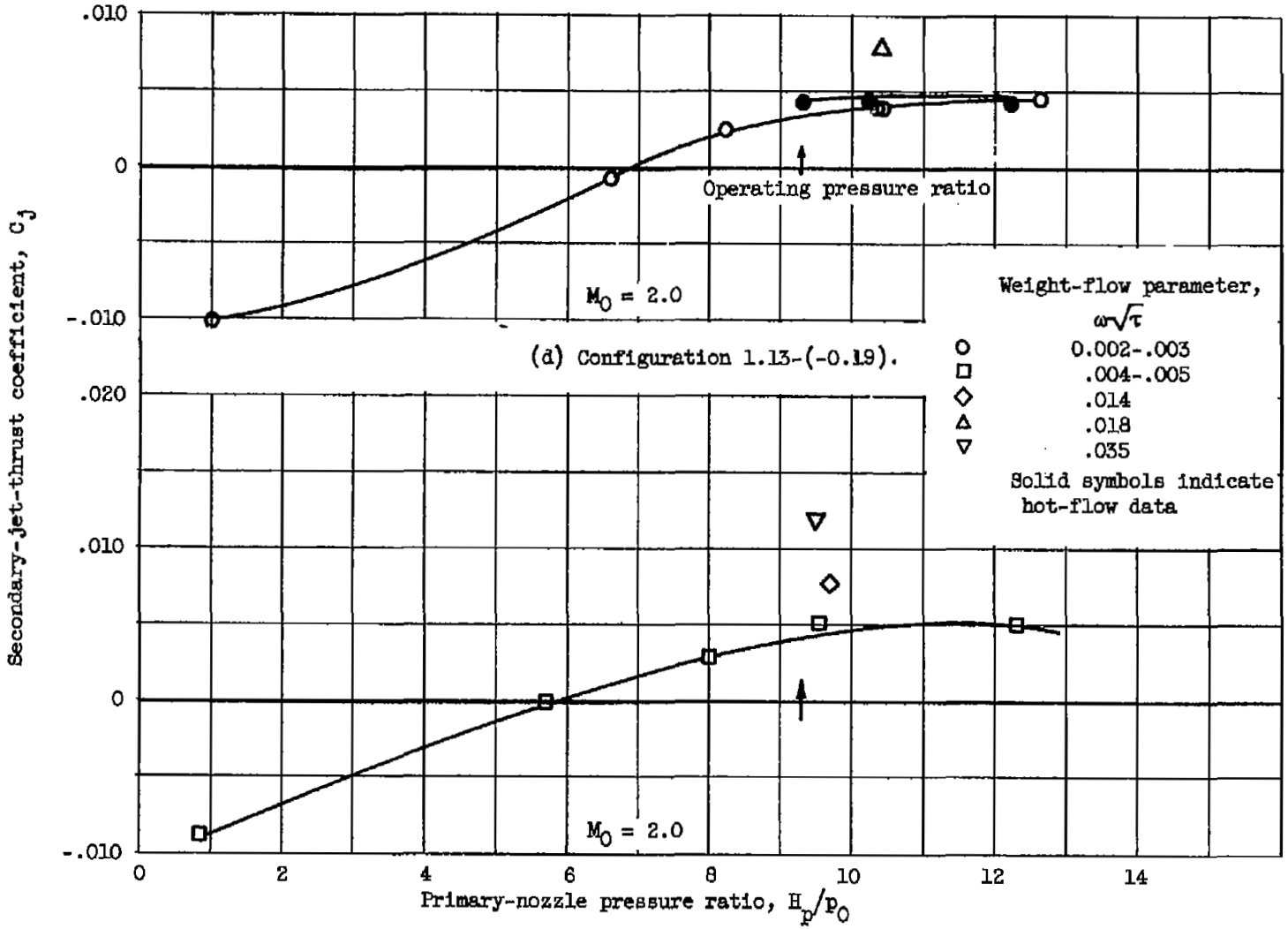

(d) Configuration 1.13-(-0.19).

(e) Configuration 1.18-(-0.14).

Figure 4. - Concluded. Secondary-jet-thrust coefficient for group B nozzles.

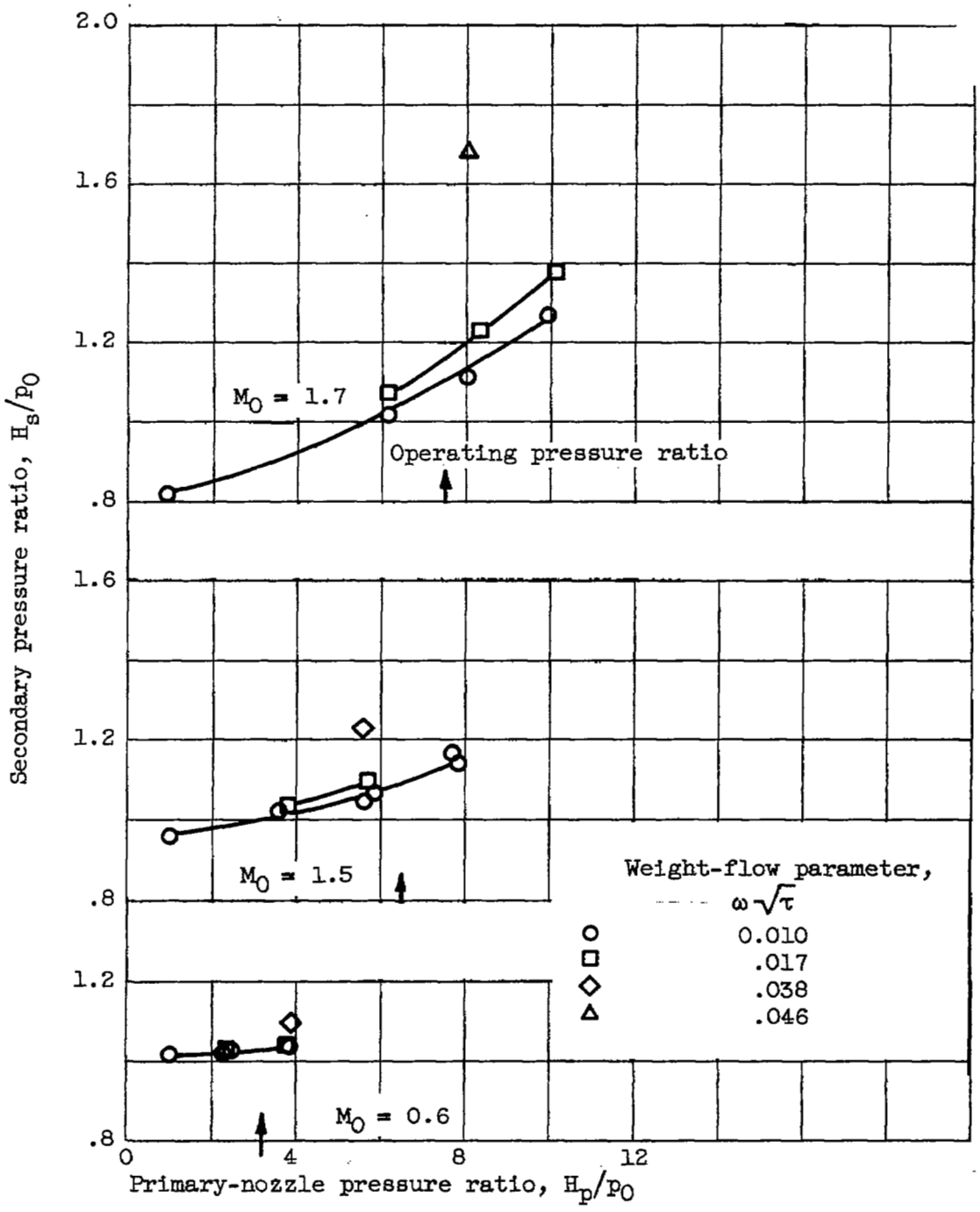

(a) Configuration 1.12-0.057.

Figure 5. - Secondary-flow characteristics of group A nozzles.

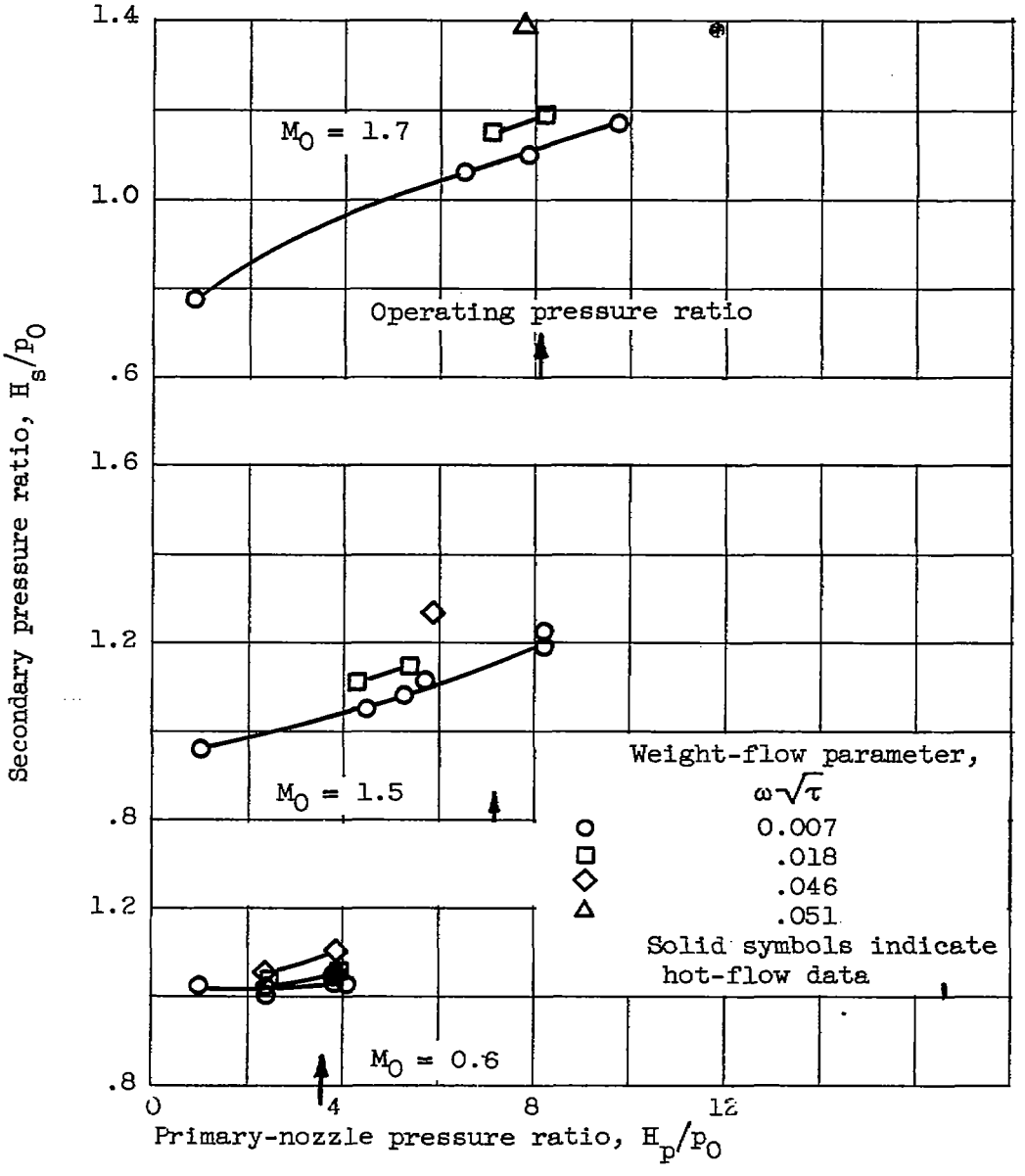

(b) Configuration 1.24-0.

Figure 5. - Continued. Secondary-flow characteristics of group A nozzles.

[redacted]

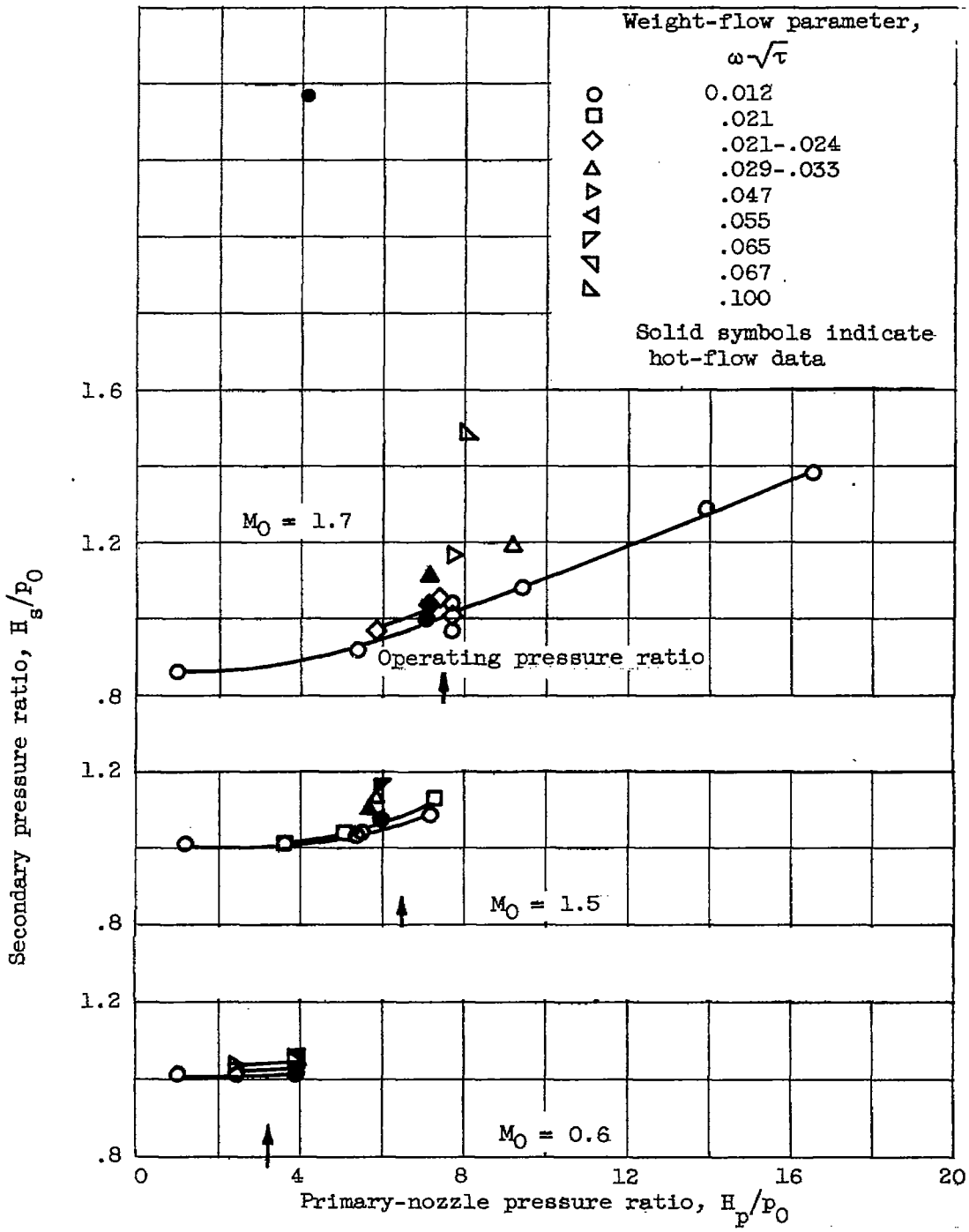

(c) Configuration 1.65-0.

Figure 5. - Concluded. Secondary-flow characteristics of group A nozzles.

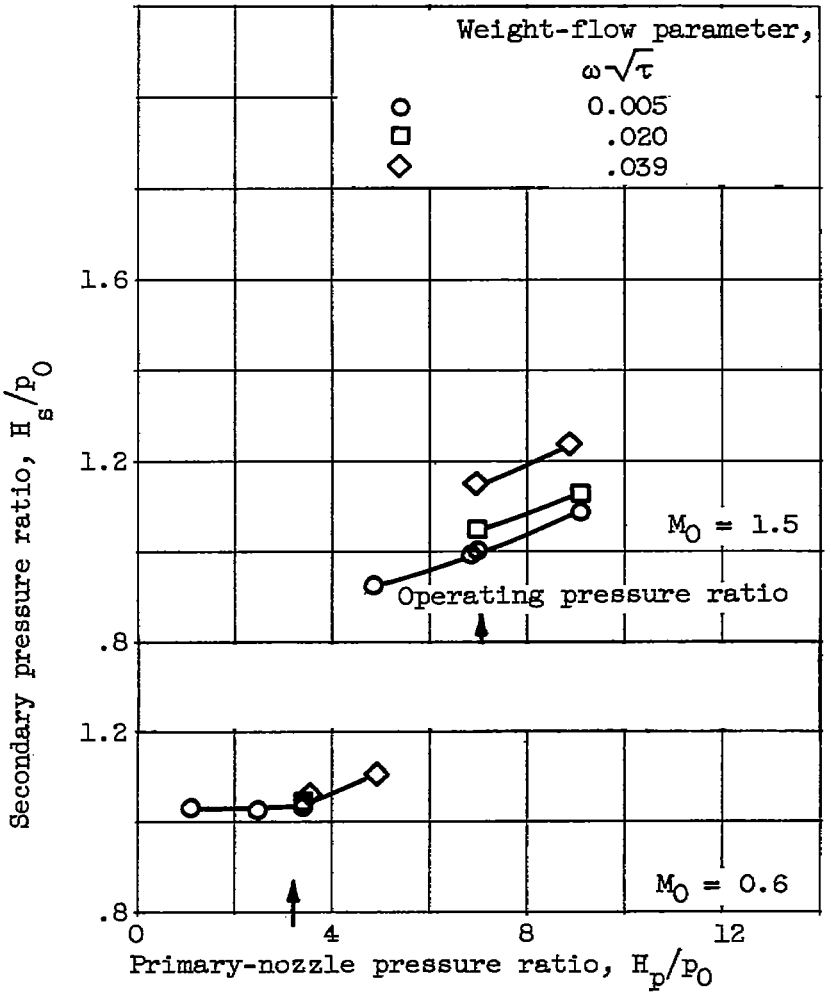

(a) Configuration 1.39-0.09.

Figure 6. - Secondary-flow characteristics of group B nozzles.

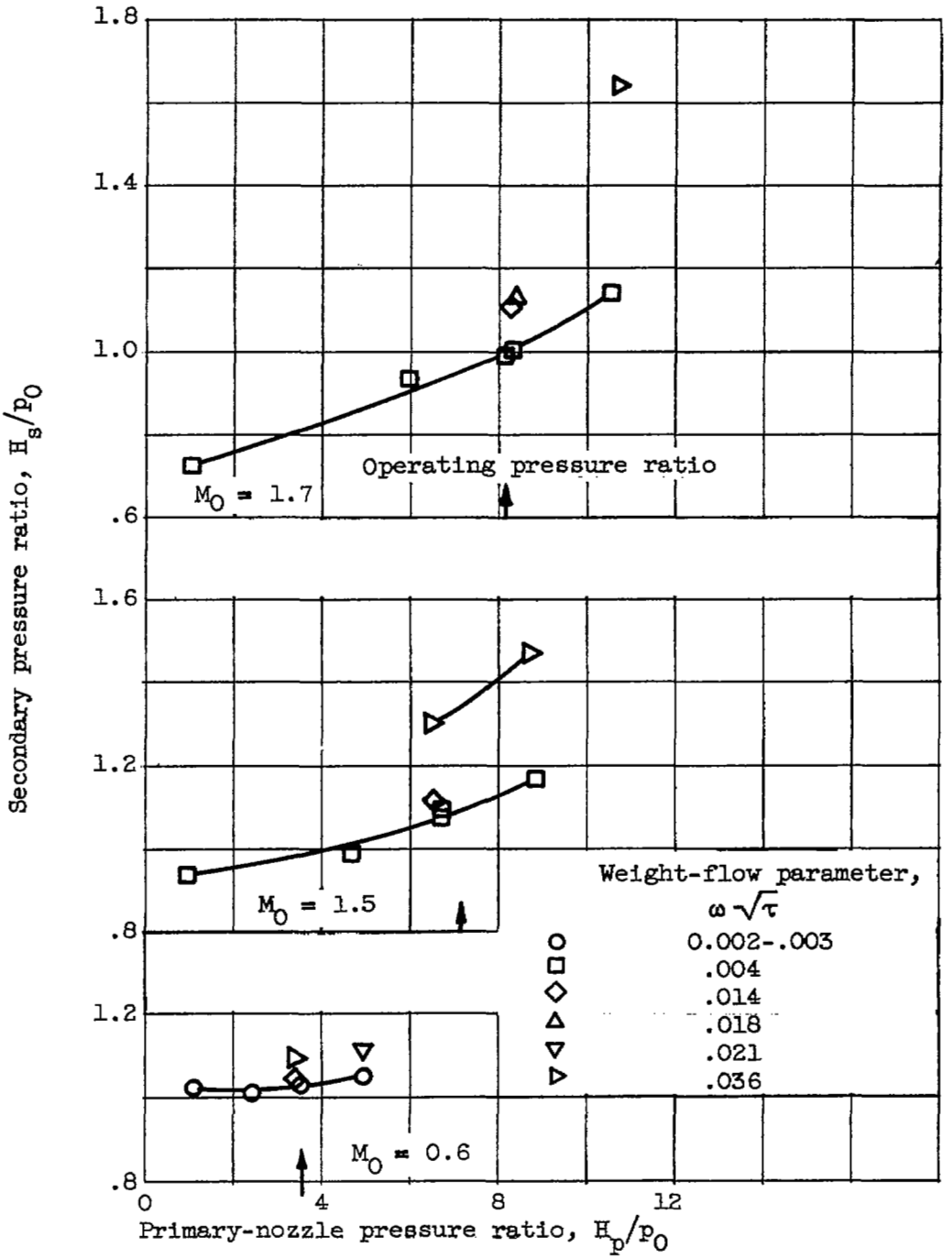

(b) Configuration 1.27-(-10).

Figure 6. - Continued. Secondary-flow characteristics of group B nozzles.

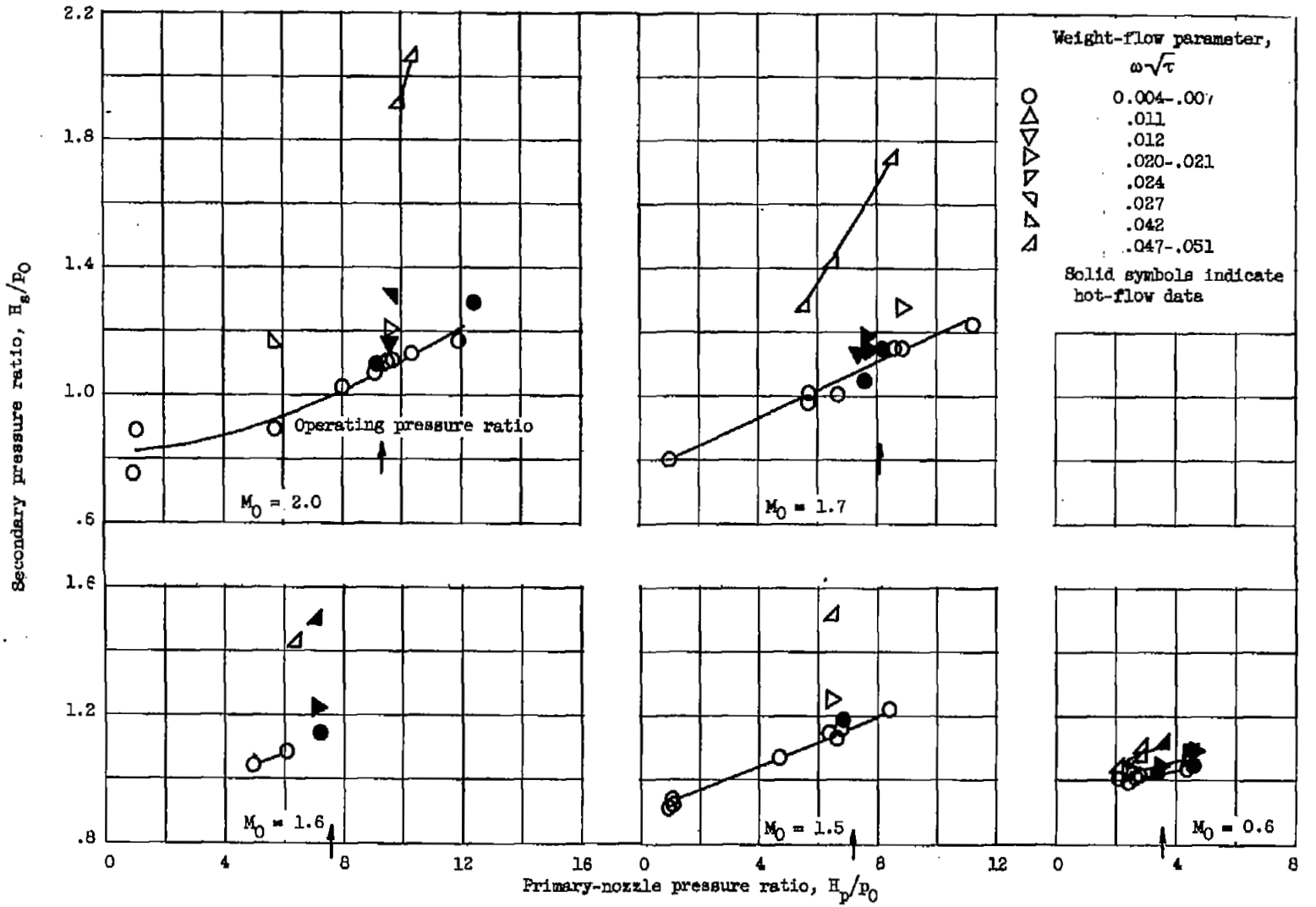

(c) Configuration 1.18-(-0.06).

Figure 6. - Continued. Secondary-flow characteristics of group B nozzles.

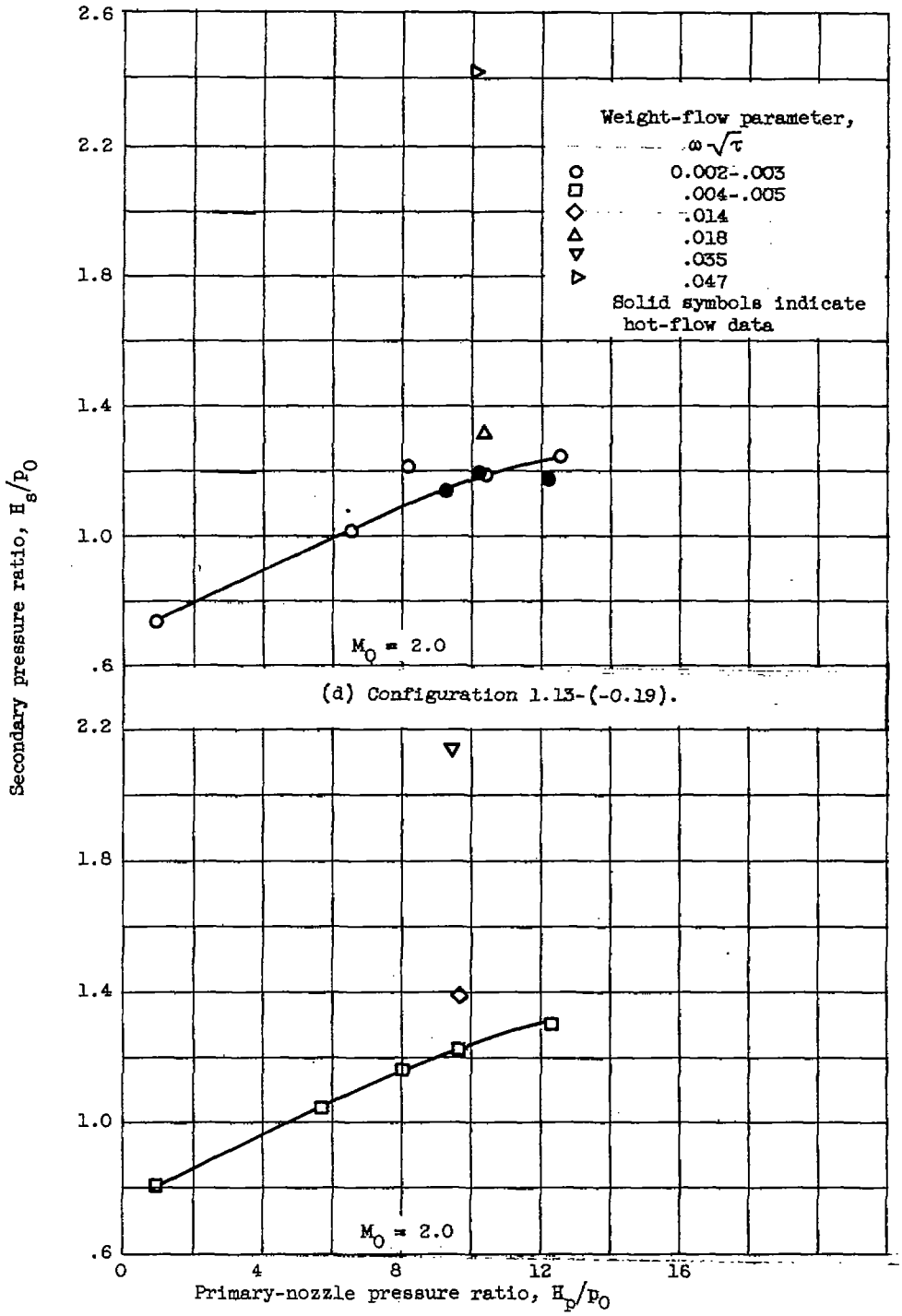

(d) Configuration 1.13-(-0.19).

(e) Configuration 1.18-(-0.14).

Figure 6. - Concluded. Secondary-flow characteristics of group B nozzles.

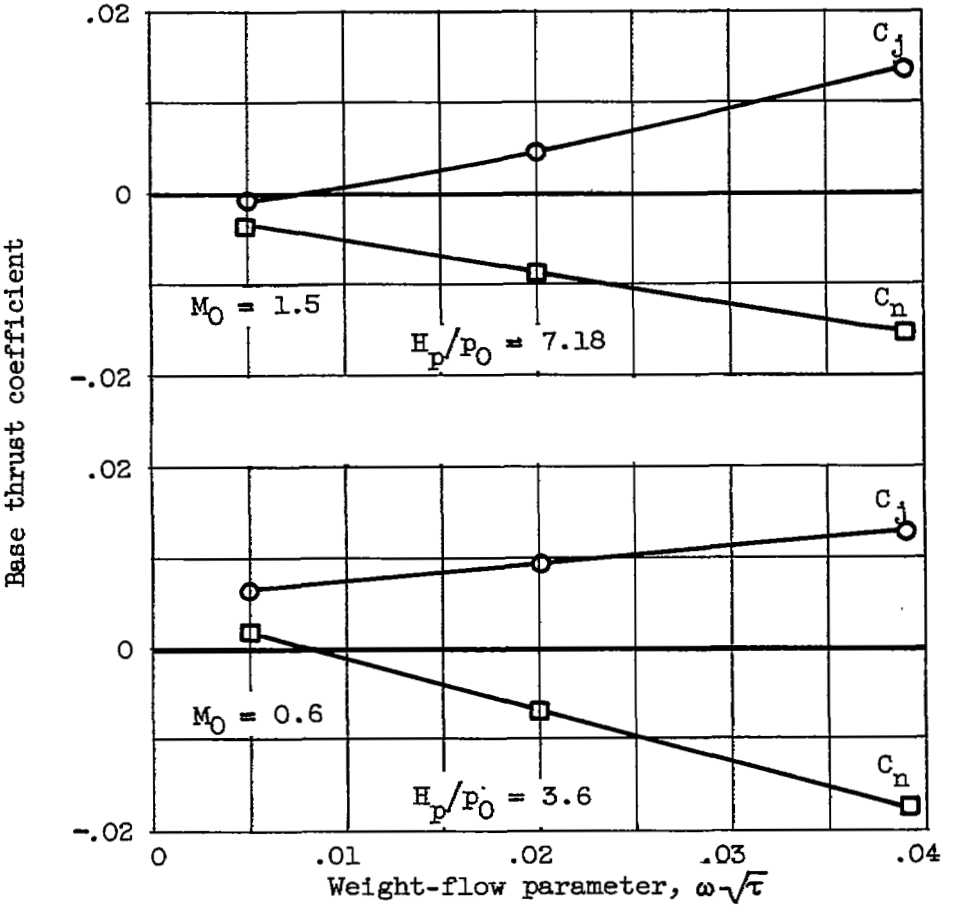

(a) Configuration 1.39-0.09.

Figure 7. - Effect of inlet momentum loss on base thrust coefficient. C_j, secondary-jet-thrust coefficient; C_n, secondary-net-thrust coefficient; M_0, free-stream Mach number; H_p/p_0, primary-nozzle pressure ratio.

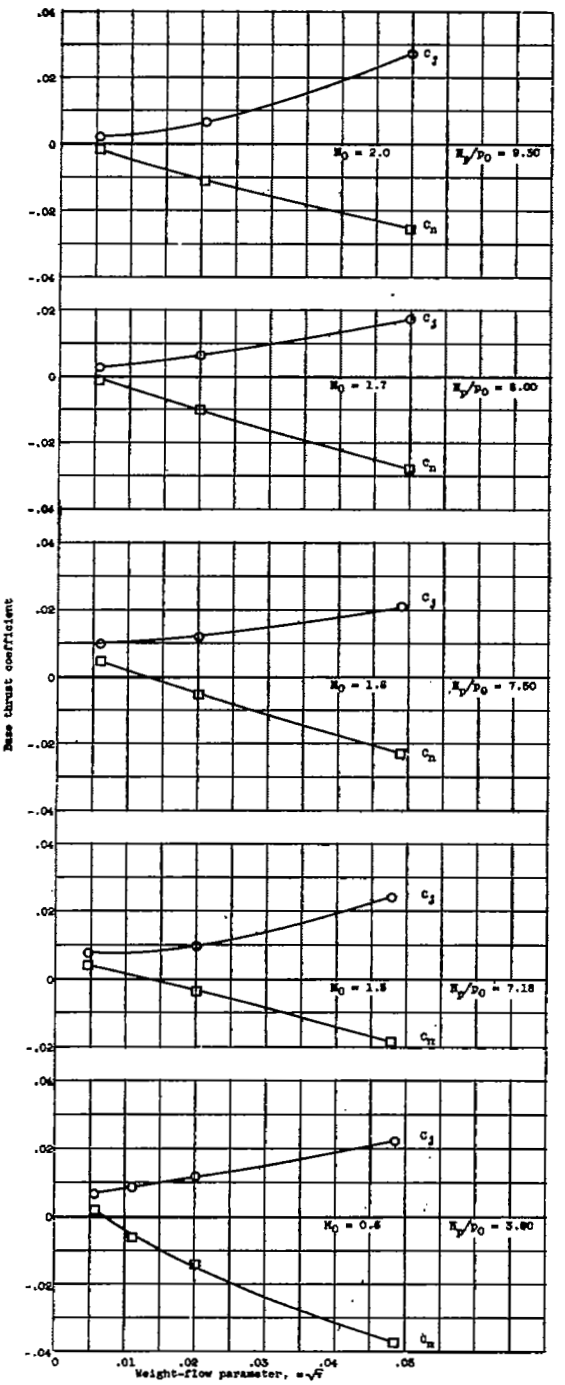

(b) Configuration 1.18-(-0.06).

Figure 7. - Concluded. Effect of inlet momentum loss on base thrust coefficient. C_j, secondary-jet-thrust coefficient; C_n, secondary-net-thrust coefficient; M_0, free-stream Mach number; H_p/p_0, primary-nozzle pressure ratio.